



# Thermodynamics of CeSiO 4: Implications for Actinide Orthosilicates

Andrew Strzelecki, Clement Bourgeois, Kyle Kriegsman, Paul Estevenon, Nian Wei, Stephanie Szenknect, Adel Mesbah, Di Wu, Rodney Ewing, Nicolas Dacheux, et al.

## ► To cite this version:

Andrew Strzelecki, Clement Bourgeois, Kyle Kriegsman, Paul Estevenon, Nian Wei, et al.. Thermodynamics of CeSiO 4: Implications for Actinide Orthosilicates. *Inorganic Chemistry*, 2020, 59 (18), pp.13174-13183. 10.1021/acs.inorgchem.0c01476 . hal-03005926

**HAL Id: hal-03005926**

**<https://hal.science/hal-03005926>**

Submitted on 16 Nov 2020

**HAL** is a multi-disciplinary open access archive for the deposit and dissemination of scientific research documents, whether they are published or not. The documents may come from teaching and research institutions in France or abroad, or from public or private research centers.

L'archive ouverte pluridisciplinaire **HAL**, est destinée au dépôt et à la diffusion de documents scientifiques de niveau recherche, publiés ou non, émanant des établissements d'enseignement et de recherche français ou étrangers, des laboratoires publics ou privés.

# Thermodynamics of CeSiO<sub>4</sub>: Implications for Actinide Orthosilicates

**Andrew C. Strzelecki**<sup>1,2,3</sup>, Clement Bourgeois<sup>1,2</sup>, Kyle W. Kriegsman<sup>1,2</sup>, Paul Estevenon<sup>4,5</sup>, Nian Wei<sup>1,6</sup>, Stephanie Szenknect<sup>4</sup>, Adel Mesbah<sup>4</sup>, Di Wu<sup>1,2,3,7</sup>, Rodney C. Ewing<sup>8</sup>, Nicolas Dacheux<sup>4</sup>, Xiaofeng Guo<sup>1,2,3,\*</sup>

<sup>1</sup> *Department of Chemistry, Washington State University, Pullman, Washington 99164, United States*

<sup>2</sup> *Alexandra Navrotsky Institute for Experimental Thermodynamics, Washington State University, Pullman, Washington 99164, United States*

<sup>3</sup> *Materials Science and Engineering, Washington State University, Pullman, Washington 99164, United States*

<sup>4</sup> *ICSM, Univ Montpellier, CNRS, CEA, ENSCM, Site de Marcoule - Bât. 426, 30207 Bagnols sur Cèze, France*

<sup>5</sup> *CEA, DES, ISEC, DMRC, Univ Montpellier, Marcoule, France*

<sup>6</sup> *College of Physical Science and Technology, Sichuan University, Chengdu 610065, People's Republic of China*

<sup>7</sup> *The Gene and Linda Voiland School of Chemical Engineering and Bioengineering, Washington State University, Pullman, Washington 99164, United States*

<sup>8</sup> *Department of Geological Sciences, Stanford University, Stanford, California 94305, United States*

---

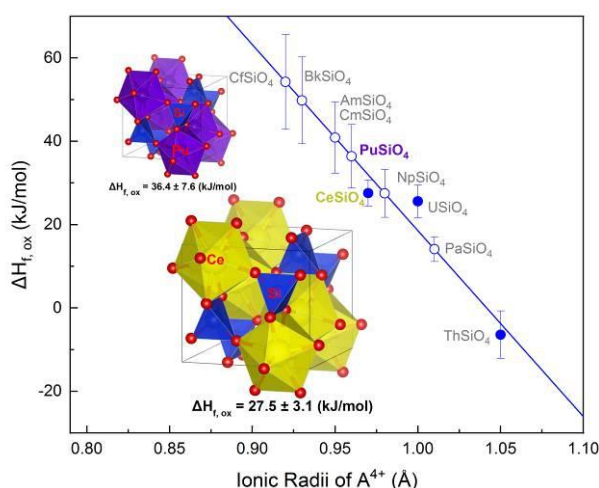
\* e-mail: x.guo@wsu.edu

## Abstract:

The mineral zircon ( $\text{ZrSiO}_4$ ;  $I4_1/amd$ ) can accommodate natural actinides, such as thorium and uranium. The zircon structure has also been obtained for several of the end member compositions of other actinides, such as plutonium and neptunium. However, the thermodynamic properties of these actinide zircon structure-types are largely unknown due to the difficulties in synthesizing these materials and handling transuranium actinides. Thus, we have completed a thermodynamic study of cerium orthosilicate, stetindite ( $\text{CeSiO}_4$ ), a surrogate of  $\text{PuSiO}_4$ . For the first time, the standard enthalpy of formation of  $\text{CeSiO}_4$  was obtained by high temperature oxide melt solution calorimetry to be  $-1971.9 \pm 3.6$  kJ/mol. Stetindite is energetically metastable with respect to  $\text{CeO}_2$  and  $\text{SiO}_2$  by  $27.5 \pm 3.1$  kJ/mol. The metastability explains the rarity of the natural occurrence of stetindite and the difficulty of its synthesis. Applying the obtained enthalpy of formation of  $\text{CeSiO}_4$  from this work, along with those previously reported for  $\text{USiO}_4$  and  $\text{ThSiO}_4$ , we developed an empirical energetic relation for actinide orthosilicates. The predicted enthalpies of formation of  $\text{AnSiO}_4$  are then made with a discussion of future strategies to efficiently immobilize Pu or minor actinides in the zircon structure.

**Keywords:** cerium orthosilicate; thermodynamics; enthalpy of formation; ceramic waste forms; rare earth minerals; actinide geochemistry; lanthanide geochemistry; stetindite

## TOC:



## Introduction:

The fate of actinides from spent nuclear fuel discharged from a reactors, the actinide-containing waste separated by chemical processing of nuclear fuels, and of plutonium from dismantled nuclear weapons has raised several daunting environmental issues<sup>1</sup>. Currently, many countries are investigating solid matrices in order to immobilize the actinides prior to permanent disposal<sup>2</sup>. The immobilization step is typically accomplished either by vitrification or cementation, while the permanent disposal is completed either by a deep-mined geologic repository or deep bore-hole<sup>3-5</sup>. The main concern with this strategy, is the long-term safety associated with a disposal system's integrity on time scales that range from thousands to hundreds of thousands of years<sup>6</sup>. The structural and chemical stability of ceramics has been ascertained by studies of minerals, such as garnet, pyrochlore, zircon, zirconolite, apatite and monazite<sup>7-15</sup> which are all known to be able to incorporate Th and U over geologic time scales that stretch well beyond a million years<sup>16</sup>. Thus, the use of these mineral structure "analogues" as potential ceramic-based waste hosts for the permanent immobilization of actinides and long lived fission products have been the subject of considerable research over the past several decades<sup>17-23</sup>.

Among the single-phase, one of the crystalline ceramic candidates for actinide immobilization is the mineral zircon ( $\text{ZrSiO}_4$ ;  $I4_1/amd$ ).<sup>13,14,24</sup> This is a direct result of zircon being an extremely durable mineral with a high loading of actinides and lanthanides<sup>25</sup>. The durability of zircon is demonstrated through its high insolubility under a variety of geochemically relevant conditions<sup>26-28</sup> (*i.e.* high P-T environments and highly saline brines), even retaining these properties of insolubility as it undergoes metamictization<sup>13,23,25</sup>, and a high physical toughness as the mineral grains are shown to endure the abrasive nature of weathering and erosional processes<sup>29</sup>.

Furthermore, zircon has been reported to readily allow for the substitution of Pu into its structure and has been identified as a key mineral phase for Pu in the "lavas" at the Chernobyl Nuclear Power Plant<sup>21,30-33</sup>. The synthesis of a pure Pu endmember orthosilicate ( $\text{PuSiO}_4$ ) possessing the zircon structure was reported in the literature by Keller in 1963 through hydrothermal synthetic techniques<sup>34</sup>, however questions still remain about the overall purity of this zircon and the extreme difficulty of such a synthesis<sup>35</sup>. Also, there could be an miscibility gap within the  $(\text{Zr,Pu})\text{SiO}_4$  system, as is evidenced by the substitution of Pu into zircon becoming increasingly more difficult when exceeding 10 wt% Pu<sup>15,36,37</sup>. This is most likely attributed to the thermodynamically unfavorable formation of  $\text{PuSiO}_4$  from its binary oxides,  $\text{PuO}_2$  and  $\text{SiO}_2$ , which also indicates the instability Pu introduces to the zircon structure for the following solid-solution reaction:  $x \text{Pu}^{4+} + \text{ZrSiO}_4 \rightarrow (\text{Pu}_x\text{Zr}_{1-x})\text{SiO}_4 + x \text{Zr}^{4+}$ . This hypothesis is supported by the recent work by Estevenon *et al.* in 2020, where they found that the

hydrothermal conditions under which a pure PuSiO<sub>4</sub> may form are extremely limited, with PuSiO<sub>4</sub> as the minor product and PuO<sub>2</sub> and SiO<sub>2</sub> being the major phases<sup>35</sup>. Thus, due to the challenge of obtaining pure PuSiO<sub>4</sub> and the safety precautions in handling of transuranium bearing orthosilicates, our experiments were conducted on CeSiO<sub>4</sub>. Cerium was selected as the surrogate for Pu, due to the similarity in structure, and the ionic radii of the A-site cations and chemical properties (*i.e.*, multiple valence states)<sup>38–41</sup>. Ce<sup>4+</sup> in the eight-coordination environment has an ionic radius of 0.97 Å, which is very close to that of eight-coordinated Pu<sup>4+</sup> (0.96 Å)<sup>42</sup>, therefore Ce in the solid-state system can be used to simulate Pu. Pure synthetic CeSiO<sub>4</sub> has been successfully prepared by both direct and indirect hydrothermal methods in 2019<sup>43,44</sup> and has been used for the thermodynamic study in this paper.

We have measured the thermodynamic property of CeSiO<sub>4</sub> for the first time. The significance is two-fold. Firstly, it has been well accepted that an empirical thermodynamic relationship exists within isostructural ceramic materials<sup>45</sup> that the enthalpy of formation ( $\Delta H_f$ ) for the ceramic phase can be correlated with the ionic radii of metal cations<sup>46</sup>. Thus, given the measured  $\Delta H_f$  of orthosilicates, one may predict  $\Delta H_f$  of an unknown phase (*i.e.* PuSiO<sub>4</sub>) through linear extrapolations<sup>47</sup>. This methodology enables the evaluation of the impact of Pu and minor actinides to the zircon structure from a thermodynamic perspective. Previously, thermodynamic parameters for coffinite (USiO<sub>4</sub>) and thorite (ThSiO<sub>4</sub>), isostructural compounds to zircon, have been determined experimentally<sup>1,8,48</sup>. Coffinite was found to be metastable, as evidenced by its positive enthalpy of formation from oxides ( $\Delta H_{f,ox} = 25.6 \pm 3.9$  kJ/mol<sup>48</sup>) measured by Guo *et al.* using the high temperature oxide melt solution calorimetry, and the positive Gibbs free energy of formation ( $\Delta G_{f,ox} = 20.6 \pm 5.2$  kJ/mol<sup>49</sup>) determined by Szenknect *et al.* from solubility studies. The metastability of coffinite directly explains the difficulty associated with its synthesis such that one cannot simply prepare coffinite by a conventional solid-state reaction<sup>50</sup>. However, thorite is relatively easier to synthesize by various solid-state and aqueous-chemistry methods<sup>51–54</sup>, despite of the ionic similarity in Th<sup>4+</sup> (1.05 Å) and U<sup>4+</sup> (1.00 Å)<sup>42</sup>, the less difficult synthesis is consistent with its negative value of  $\Delta H_{f,ox}$ ,  $-6.4 \pm 5.7$  kJ/mol<sup>8</sup>. Additionally, Ferriss *et al.* in 2010 performed density functional theory (DFT) calculations<sup>37</sup> to predict  $\Delta H_f$  of CeSiO<sub>4</sub>, ThSiO<sub>4</sub>, USiO<sub>4</sub>, and PuSiO<sub>4</sub>. The DFT results predict values in good agreement with those of ThSiO<sub>4</sub><sup>8</sup>, USiO<sub>4</sub><sup>48</sup>, and CeSiO<sub>4</sub> from this work.

Secondly, the natural mineral occurrence of CeSiO<sub>4</sub>, stetindite, was discovered in 2009 in a granitic pegmatite in Norway<sup>55</sup>. However, there are no studies of its thermodynamic stability. Thus, the first determination of  $\Delta H_f$  for CeSiO<sub>4</sub> provides a basis for understanding the geochemical factors leading to the formation of this relatively rare mineral.

## 2. Experimental Methods

### 2.1. Sample synthesis and characterization:

CeSiO<sub>4</sub> samples were synthesized by hydrothermal method from Ce(III)-silicate solid precursor according to the protocol described by Estevenon *et al.*<sup>44</sup>. A stoichiometric mixture of CeO<sub>2</sub> (Sigma Aldrich, particle size < 5 μm) and SiO<sub>2</sub> (Sigma Aldrich, 10-20 nm) were mechanically milled (30 Hz, 1 hour) with a Retsch MM 200 vibration mill mixer in a tungsten carbide milling vessel. This mixture was pelletized by uniaxial pressing under 5 MPa at room temperature and then heated at 1350°C under reductive atmosphere (Ar-4% H<sub>2</sub>) to prepare A-Ce<sub>2</sub>Si<sub>2</sub>O<sub>7</sub> (tetragonal system, space group *P4<sub>1</sub>*). 200 mg of A-Ce<sub>2</sub>Si<sub>2</sub>O<sub>7</sub> was placed in contact with 4 mL of a 0.75 M HNO<sub>3</sub> solution (prepared by dilution of ACS grade 70% HNO<sub>3</sub>, Sigma Aldrich), the pH of that solution was then adjusted to 7.0 using freshly prepared NaOH solution (from ACS grade NaOH pellets, Sigma Aldrich). This mixture was hydrothermally treated for 7 days at 150°C under air atmosphere in a 23 mL Teflon lined Parr autoclaves. The final product was separated from the aqueous solution by centrifugation, washed twice with deionized water and once with ethanol and then dried overnight at 60°C. The final CeSiO<sub>4</sub> powder sample was well characterized by a multitude of different characterization techniques. A summary of the techniques and the resulting data are presented in the supplementary information (SI) to this manuscript, with a more detailed description of the characterization being found in our previous work of Estevenon *et al.* 2019<sup>44</sup>. These techniques included XRD (Figure S1), FTIR (Figure S2), Raman (Figure S3), XANES (Figure S4), EXAFS (Figure S5) and SEM (Figure S6). The results of all of these techniques allows us to confirm that the material which was investigated through the calorimetric techniques utilized and presented in this study to be chemically CeSiO<sub>4</sub>, with all the Ce presented being tetravalent, and the overall structure to belong to the space group *I4<sub>1</sub>/amd*.

### 2.2. Thermogravimetric analysis coupled with differential thermal analysis (TGA-DTA):

The TGA-DTA measurements were performed on a Setaram SetSYS 2400 thermogravimetric differential scanning calorimeter, where CeSiO<sub>4</sub> was heated from 28°C to 1200°C, with a heating rate of 10°C/min., under a flowing N<sub>2</sub> atmosphere (20 mL/min.). The temperature and sensitivity of the instrument was calibrated by heating indium, tin, lead, zinc, and aluminum across their fusion point repeatedly at the temperature change rates of 5, 10, 15, and 20°C/min. The signals of each phase transition were then calibrated against the known heats of fusion for the metals.

### 2.3. High temperature oxide melt solution calorimetry:

The enthalpy of drop solution ( $\Delta H_{ds}$ ) was directly measured by a Setaram AlexSYS-1000 Calvet-type calorimeter. The calibration of the instrument was conducted by performing transpose temperature drops using solid pieces of  $\alpha$ -Al<sub>2</sub>O<sub>3</sub> and Pt. Powdered samples were hand pressed into pellets, with masses between 3-5 mg, and dropped from room temperature into a molten solvent of sodium molybdate (Na<sub>2</sub>O·MoO<sub>3</sub>) contained in a Pt crucible at 700°C. The calorimeter chambers were continuously flushed with O<sub>2</sub> gas at a rate of ~100 mL/min in order to facilitate a constant gas environment above the solvent. The Na<sub>2</sub>O·MoO<sub>3</sub> melt is slightly oxidative<sup>56,57</sup> and will maintain a redox environment which will keep all of the dissolved Ce in melt as Ce<sup>4+</sup>.<sup>58-60</sup> Flushing of O<sub>2</sub> gas above the solvent also further aids in maintaining an oxidative solvent environment, by oxidizing any low-valence Mo to Mo<sup>+6</sup>. Further, the Na<sub>2</sub>O·MoO<sub>3</sub> solvent dissolves refractory elements, such as Ce, but is relatively chemically inert to silicon (Si)<sup>48,58,60,61</sup>. Therefore, the solvent saturation method<sup>62</sup> was used for correctly accounting for the energy associated with the all Si in the stetindite. This was accomplished by saturating 15g of Na<sub>2</sub>O·MoO<sub>3</sub> with 100 mg of silica gel prior to the experiments as the solvent will no longer dissolve any SiO<sub>2</sub>, but instead will precipitate out as cristobalite at 700°C. All of the calibration and methodology employed in this study are further described in more detail in previous reports<sup>11,48,58,62-65</sup>. Associated

## 3. Results & Discussion

### 3.1. Thermogravimetric analysis coupled with differential thermal analysis (TGA-DTA):

Thermogravimetric analysis (TGA) of CeSiO<sub>4</sub> showed two mass losses (Figure 1). The first mass loss of 3.20% occurs from room temperature to 900°C and is associated with the removal of surface water and structural water. The water content of the synthetic CeSiO<sub>4</sub> was quantified from the TGA result leading to the chemical formula: CeSiO<sub>4</sub>·0.43H<sub>2</sub>O, which also resembles the hydrated form of synthetic USiO<sub>4</sub> prepared by hydrothermal methods<sup>48</sup>. The origins and location of water within zircon structural materials has been highly debated in the literature<sup>17,52,66-71</sup>. The observation of a continual mass till 900°C, shows that majority of the water associated with CeSiO<sub>4</sub> is energetically strongly associated with the material, for merely adsorbed surficial water would leave the sample below 200°C. This conclusion of strongly associated water is consistent with the previous observations of excess water associated with both natural and synthetic coffinite samples (USiO<sub>4</sub>).<sup>17,48</sup> However, the origins of such excess water in coffinite is

not simple and still subject to debate as both infrared spectroscopic and X-ray diffraction studies have ruled out the water being structural<sup>17,52,66–70</sup>. One prevailing theory of how water is associated with natural zircons is in form of OH- and various Zr or Si related vacancies<sup>71</sup>. Such OH- groups would be evident in the 3000-3500cm<sup>-1</sup> IR region<sup>72</sup> of which was not detected by FTIR (Figure S2) and would further require a charge substitution of Ce<sup>4+</sup> to Ce<sup>3+</sup>, which was not present in the XANES spectra (Figure S4). Lastly, the EXAFS (Figure S5) of the material elucidates that the coordination environment of the elements is that of a zircon structural material, with no vacancies or OH- being found to contribute. A potential origin of water which is energetically strongly associated, but non-structural, and is not readily visible through FTIR or XRD could be as confined molecular water inside channels along the [001] in the zircon structure<sup>17,70,73</sup>. This hypothesis offers an explanation for why the water is observed as molecular and not structural<sup>69</sup>.

The second mass loss (2.17%) from 980 - 1110°C corresponds to ¼ of a mole of O<sub>2</sub> being released in association with the reduction of Ce<sup>4+</sup> to Ce<sup>3+</sup> resulting in the cerium (III) disilicate phase, A-Ce<sub>2</sub>Si<sub>2</sub>O<sub>7</sub> under the inert atmosphere. This is further supported by the corresponding endothermic heat flow indicated by DTA. The decomposition temperature is much higher than 700°C at which the oxide melt solution calorimetry was conducted. Thus, we conclude that the decomposition has no bearing to the final thermochemical results.

### 3.2. Enthalpy of formation of CeSiO<sub>4</sub>:

The hydrothermally prepared CeSiO<sub>4</sub> sample used in this study exhibits a similar hydrated composition to that of the analogous synthetic USiO<sub>4</sub> prepared by similar hydrothermal techniques<sup>48,74</sup>. To ensure the quality of the obtained enthalpy of formation, we followed the previously developed methodology for hydrated minerals (*e.g.*, coffinite<sup>48</sup>) and performed two sets of high-temperature oxide melt solution calorimetry experiments. The first set of these experiments were performed using the sample as is, with a chemical formula of CeSiO<sub>4</sub>·0.43H<sub>2</sub>O. Through these experiments the enthalpy of drop solution ( $\Delta H_{ds}$ ) of CeSiO<sub>4</sub>·0.43H<sub>2</sub>O was found to be 95.36 ± 3.52 kJ/mol (Table 1). The second set of experiments was done after the sample was fully dehydrated. The dehydration of the sample was accomplished by heating pelletized samples (3-5 mg) for two hours under an inert atmosphere of N<sub>2</sub> to 800°C. Samples were then stored at room temperature under a N<sub>2</sub> atmosphere prior to being dropped in order to avoid any potential water re-adsorption. All of the experimental parameters and materials exactly mirrored those utilized for the hydrated sample outlined above in the methods sections. The resulting enthalpy of

drop solutions determined by these experiments was  $\Delta H_{ds} = 92.88 \pm 3.40$  kJ/mol (Table 1), slightly less endothermic than that from the first experiment. This is reasonable because the thermal dehydration leads to the positive contribution to the  $\Delta H_{ds}$  value. However, the difference, 2.48 kJ/mol, is unexpectedly small. The small hydration enthalpic value could be due to the partial dehydration of  $\text{CeSiO}_4 \cdot 0.43\text{H}_2\text{O}$  during dropping before it reached the reaction chamber where the measurements were taken. AlexSYS-1000 has an inhomogeneous temperature profile, with over 60 cm above the reaction chamber maintaining at around 650°C. Rapid dehydration could occur,<sup>75,76</sup> and the composition of the resulting sample detected by the thermopiles was estimated from the TGA result to be  $\text{CeSiO}_4 \cdot 0.025\text{H}_2\text{O}$ .

The  $\Delta H_{ds}$  for such partially hydrated sample must be then corrected in order to account for the additional energetics related with the associated water. As it was stated above, it is reasonable to assume that a portion of water is strongly bonded to  $\text{CeSiO}_4$  as the TGA data showed an extended mass loss till 900°C. Using an integral adsorption enthalpy of -80 kJ/mol per mol of  $\text{H}_2\text{O}$  (-44 kJ/mol for “free water”) for the adsorbed water, which was observed in the alumina and titania<sup>77–79</sup> and used for estimating hydration energy of coffinite<sup>48</sup>, one may derive the corrected  $\Delta H_{ds}$  for anhydrous  $\text{CeSiO}_4$  to be  $88.7 \pm 3.4$  kJ/mol and  $\Delta H_{f,ox}$  to be  $29.2 \pm 3.5$  kJ/mol (Table 1). While the direct measurement of anhydrous  $\text{CeSiO}_4$  yields  $\Delta H_{f,ox}$  of  $25.0 \pm 3.5$  kJ/mol (Table 1), by averaging the results of the two experiments,  $\Delta H_{f,ox}$  of  $\text{CeSiO}_4$  reaches  $27.5 \pm 3.1$  kJ/mol (Table S1), which is in excellent agreement with the DFT predicted value, 23.8 kJ/mol<sup>37,63</sup>. With all of the evidence supporting that water is energetically strongly associated with stetindite, we report that  $\Delta H^\circ_f = -1971.9 \pm 3.6$  kJ/mol, which is first reported standard enthalpy of formation data of stetindite (Table S1).

### 3.3. Energetic Landscape of End-Member Actinide orthosilicates:

Several empirical methodologies were developed for the prediction thermodynamic parameters of ceramic compounds. For instance, Chen *et al.* discovered that both the Gibbs free energies ( $\Delta G_f$ ) and enthalpies of formation ( $\Delta H_f$ ) of hexavalent uranium minerals could be predicted through the structural-summation technique.<sup>80</sup> Whereas, Sverjensky and Molling<sup>45</sup> established an empirical linear relationship between the free energy of isostructural inorganic solids and the ionic radii of aqueous metal cations. While this model was originally developed for divalent cations the model has been expanded to include tetravalent cations and its application allowed for the free energies of crystalline solids to be estimated by only having experimental data on a few samples.<sup>81,82</sup> A very similar empirical linear relationship has been recognized for

isostructural inorganic compounds which links the enthalpies of formation with the ionic radii of metal cations.<sup>46</sup> Many lanthanide and actinide bearing isostructural ceramic materials follow this empirical trend and it has been applied numerous times in the literature<sup>47,64,83–85</sup>.

By using the experimentally determined  $\Delta H_{f,ox}$  of  $\text{CeSiO}_4$  ( $27.5 \pm 3.1$  kJ/mol),  $\text{USiO}_4$  ( $25.6 \pm 3.9$  kJ/mol<sup>48</sup>) and  $\text{ThSiO}_4$  ( $-6.4 \pm 5.7$  kJ/mol<sup>8</sup>) and the ionic radii ( $\text{\AA}$ ) of metal cations in an eight-fold coordination environment<sup>42</sup>, a near linear trend is found between  $\Delta H_{f,ox}$  and the ionic radius  $r$  ( $\text{\AA}$ ),  $\Delta H_{f,ox} = (-446.3 \pm 152.5) r - (464.9 \pm 153.6)$ , with an adjusted  $R^2 = 0.79096$ . From the obtained linear regression, we obtained the  $\Delta H_{f,ox}$  for the other actinide (Pa, Np, Pu, Am, Cm, Bk, Cf) orthosilicates (Figure 2). The heavier transuranic elements (Am, Cm, Bk, and Cf) show more lanthanide-like characteristics, thus prefer having a trivalent oxidation state<sup>86–88</sup>. The trivalent oxidation would result in different ionic radii and preferred coordination chemistry<sup>89,90</sup>. In order for such trivalent cations to be introduced into the zircon structure a charge-coupled substitution would be required. Nonetheless, the tetravalent states of all the aforementioned elements are possible through either a transient state as a result of radiation-induced radiolysis<sup>91–93</sup> or a steady state being stabilized by either ligands or electrochemical methods<sup>88,94–96</sup>. Each of these states, the transient state and steady state conditions, are achievable in the unlikely event of a failure of the geological repository and breach in radiological waste canister. Each of these states could be observed under such a hypothetical scenario, if said geological repository is located in a geologic setting where the host lithology is also rich with mineral halides (*i.e.* halite), such as what is observed at the Waste Isolation Pilot Plant (WIPP) located in New Mexico, U.S.A.<sup>97,98</sup>, then there would be a supply of radiation, heat, high ionic-strength aqueous solutions<sup>99</sup>, and silica source from the bentonite backfill<sup>100</sup>. This could cause for the dissolution of another ceramic waste form and allow for the formation of an actinide orthosilicate, with such hypothetical conditions being similar to those used in synthesizing  $\text{PuSiO}_4$ <sup>35</sup>. These actinide orthosilicate could form as colloid allowing for them to be transported immense distances<sup>101–103</sup>. Thus, here we consider the possible tetravalent states of these heavy transuranic elements and their potential impact to the structural stability.

As the thermodynamic stability of any given material is dictated by  $\Delta G_f$ , one needs  $\Delta G_f = \Delta H_f - T\Delta S_f$ , with knowing the appropriate entropy ( $\Delta S_f$ ) value besides  $\Delta H_f$ , in order to evaluate the overall stability. However, under the standard condition ( $T = 25^\circ\text{C}$ ,  $P = 1\text{Bar}$ ), the entropic term is small. This is evidenced taking coffinite as an example.  $\Delta G_f$  of coffinite was determined through solubility studies to be  $-1867.6 \pm 3.2$  kJ/mol<sup>49</sup> and its  $\Delta H_f$  was determined by high temperature drop oxide melt calorimetry to be  $-1970.0 \pm 4.2$  kJ/mol<sup>48</sup>. At  $25^\circ\text{C}$ ,  $T\Delta S_f$  equal to  $-0.344$

$\text{kJ/mol}\cdot\text{K} \times 298.15 \text{ K} = 102.6 \text{ kJ/mol}$ . Hence, under the standard condition enthalpy alone can be used to approximately discuss the stability of actinide orthosilicates and represent the energetic landscape (Figure 2). The regression of measured  $\Delta H_{f, \text{ox}}$  leads to an almost linear trend. The extrapolated results based on such linear trend are in good agreement with those reported in a previous computational study<sup>37</sup>. The result of the linear regression is summarized in Table 2 and plotted in Figure 2. Only  $\text{ThSiO}_4$  has a negative formation enthalpy ( $-6.4 \pm 5.7 \text{ kJ/mol}$ )<sup>8</sup>, while all others are expected to be thermodynamically metastable with respect to their binary oxides ( $\text{AnO}_2$  and  $\text{SiO}_2$ ). The favorable formation of  $\text{ThSiO}_4$  could be a result of its lowest ionic potential ( $Z/r$ ) of 3.81 that allows  $\text{Th}^{4+}$  to be stabilized in the zircon structure. Whereas,  $\text{USiO}_4$ ,  $\text{CeSiO}_4$ , and  $\text{PuSiO}_4$  having larger ionic potentials of 4.00, 4.12, and 4.17, respectively, and thus can destabilize the zircon structure. Said that,  $\Delta H_{f, \text{ox}}$  of  $\text{ThSiO}_4$  does follow the linear trend established in this work and does not exhibit as an exception to the general rule.

The prediction in Figure 2 are consistent with the reported difficulty in synthesizing pure  $\text{PuSiO}_4$ <sup>35</sup>, which has a predicted  $\Delta H_{f, \text{ox}}$  value of  $36.4 \pm 7.6 \text{ kJ/mol}$ . These results indicate that if one plans to use the zircon structure for immobilizing Pu or other minor actinides, they need to target synthesis strategies which disfavor the formation of binary oxides. As both coffinite and stetindite are found to have positive  $\Delta H_{f, \text{ox}}$ , the synthetic conditions of their formations could be highly informative for such strategies. Both of them have been discovered in nature under hydrothermal conditions and their synthetic analogs have been prepared by tailoring synthetic routes to avoid the formation of thermodynamically more favorable binary oxides<sup>43,44,50,53,104</sup>. In particular the formation of stetindite under laboratory conditions<sup>43,44</sup>, as the kinetics needed in order to oxidize either the  $\text{Ce}^{3+}$  intermediate complex<sup>43</sup> or  $\text{Ce}^{3+}$  solid<sup>44</sup>, into the  $\text{Ce}^{4+}$  solid were only stable under hydrothermal conditions. In addition, taking the  $\Delta H_{f, \text{ox}}$  calculated through the linear regression, we also report the predicted  $\Delta H_f^\circ$  values for  $\text{PaSiO}_4$ ,  $\text{NpSiO}_4$ ,  $\text{PuSiO}_4$ ,  $\text{AmSiO}_4$  and etc. (Table 2) by using  $\Delta H_f^\circ$  of the respected  $\text{AnO}_2$ <sup>105</sup> as the auxiliary data. The overall  $\Delta H_{f, \text{ox}}$  is shown to be thermodynamically unfavorable for the major transuranic elements, Np, Pu, Am, and Cm. Nevertheless, Am-orthosilicate has been successfully synthesized and reported by Keller in 1963,<sup>34</sup> which make  $\text{CmSiO}_4$  also highly possible to exist because of their almost identical predicted formation enthalpies.

The zircon structure-type includes other crystalline ceramics and mineral orthosilicates. The lanthanide orthovanadate ( $\text{LnVO}_4$ ) minerals wakefieldite and dreyerite, the heavy rare earth orthophosphate ( $\text{HREEPO}_4$ ) mineral xenotime, and the lanthanide orthoarsenate ( $\text{LnAsO}_4$ ) mineral chernovite all share the zircon structure<sup>17</sup>. As the orthophosphate and orthovanadate materials

enthalpies of formation have been reported in the literature<sup>59,106</sup>, they were also included in Figure 2 in order to detect any other trends across the isostructural family. This led to another important observation of the energetic landscape of orthosilicates in that both zircon and hafnion (HfSiO<sub>4</sub>) are “outliers” of the predicted trend. We hypothesize that there could be a separate trend for transitional metal orthosilicates due to the structural difference that both of Zr<sup>4+</sup> and Hf<sup>4+</sup> are smaller cations (0.84 Å and 0.83 Å, respectively). This is further supported by both of these materials following the orthovanadate trend line, which are comparable in both energetics and unit cell volume to ScVO<sub>4</sub>. This observation, however, does not exclude the possibility of zircon and hafnion being outliers as a result of the fundamental bonding difference in *d*-orbitals vs. *f*-orbitals<sup>107</sup>. Lastly, these two trends for transition metal and lanthanide/actinide orthosilicates disagree with the previously reported actinide orthosilicate energetic landscape<sup>108</sup>. The discrepancy is attributed to an inaccuracy of  $\Delta H_{\text{ds}}$  for thorite as a result of incomplete dissolution of the single crystal sample and the inconclusive  $\Delta H_{\text{ds}}$  for coffinite in the early experiments, which we have discussed in a previous work<sup>48</sup>. The experimentally derived energetic trend fully agrees with the calculated values reported by the DFT-LDA study<sup>37</sup> (Figure 2), which likewise shows that both zircon and hafnion deviate from the linear trend.

#### 3.4. Strategic analysis of immobilizing Pu or other actinides in zircon structure:

Although the pure actinide orthosilicate endmembers were calculated to have a positive  $\Delta H_{\text{f, ox}}$ , it should be investigated whether any intermediate compositions from MSiO<sub>4</sub> (M = Zr, Hf) and AnSiO<sub>4</sub> (An = Th, U, Np, Pu, etc.) endmembers can lead to thermodynamically favorable solid solutions for waste form applications. Using MSiO<sub>4</sub>-based solid solutions to strategically accommodate actinides has advantages in two different ways. Firstly, it may allow for easier synthesis of actinide-containing orthosilicates, as there could be a potential for short-range cation ordering that could significantly lower the enthalpic penalty for introducing An<sup>4+</sup> into ZrSiO<sub>4</sub>. Such a phenomenon has already been demonstrated in uranothorite solid solution (Th<sub>1-x</sub>U<sub>x</sub>SiO<sub>4</sub>), where the intermediate compositions are stabilized by a negative heat effect of -118.7 kJ/mol<sup>8</sup>. Secondly, the application of HfSiO<sub>4</sub> as the endmember, instead of ZrSiO<sub>4</sub>, can offer an additional benefit to the waste form as hafnium is a neutron absorber<sup>14,19</sup>. The soft hydrothermal synthesis of hafnion could easily be modified to incorporate tetravalent actinides<sup>109</sup>. This soft hydrothermal synthetic technique could also be scalable for industrial application<sup>110</sup>. Unfortunately, the introduction of hafnium as a neutron absorber does not imply a reduction in the susceptibility to radiation damage<sup>21</sup>, a topic that has been extensively studied in the past<sup>31,111–116</sup> and is still one of

the greatest challenges to the utilization of zircon-based ceramic as a nuclear waste host. However, the introduction of hafnium could allow the incorporation of higher loadings of radionuclides with high specific activity (e.g. plutonium and americium isotopes) in the waste form without any worry of possible criticality<sup>15</sup>.

## 5. Conclusions

Through thermogravimetric analysis, differential thermal analysis (TGA-DTA), and high temperature oxide melt solution calorimetry, the thermodynamic parameters of stetindite (CeSiO<sub>4</sub>) were determined. The results of the TGA-DTA show that CeSiO<sub>4</sub> is hydrated, similar to that of USiO<sub>4</sub><sup>48</sup>. By performing high temperature oxide melt solution calorimetry on CeSiO<sub>4</sub>, we determined its enthalpy of formation to be  $\Delta H_{f,ox} = 27.5 \pm 3.1$  kJ/mol, confirming its metastability with respect to its binary oxides. The strong endothermic heat of formation accounts for the difficulty in synthesizing this phase in addition to the overall rarity of stetindite in nature. The overall enthalpy of formation was found to be thermodynamically favorable:  $\Delta H^\circ_f = -1971.9 \pm 3.6$  kJ/mol. Exploiting the empirically derived linear trend between the enthalpy of formation and the ionic cation radius enabled the prediction of  $\Delta H^\circ_f$  of some unknown actinide silicates AnSiO<sub>4</sub> (An = Np, Pu, Am, Cm, Bk, and Cf). These high endothermic formation enthalpies provide an explanation for the difficulties in their synthesis, particularly the attempts to obtain pure PuSiO<sub>4</sub>, which was encountered by Estevenon *et al.*<sup>35</sup> using hydrothermal methods. Indeed, it appears to be difficult according to a predicted value of  $\Delta H_{f,ox} = 36.4 \pm 7.6$  kJ/mol. Furthermore, the synthesis of minor actinides possessing the zircon structure, such as AmSiO<sub>4</sub>, should be even more difficult to synthesize as they are all found to be more energetically uphill than PuSiO<sub>4</sub>, with all being estimated to have  $\Delta H_{f,ox} > 40$  kJ/mol. Lastly, we propose that some Zr-An or Hf-An orthosilicate systems may be thermodynamically favored by possible negative mixing enthalpies due to the short-range ordering of the two metal cations that can be engineered to increase the loadings of actinides in the zircon or hafnon structure-type, which have a relatively large stability field.

## Acknowledgements

This work was supported by the institutional funds from the Department of Chemistry at Washington State University. A.C.S., K.W.K, and X.G. acknowledge the support by the U.S. Department of Energy, Office of Nuclear Energy, grant DE-NE0008582. C.B. acknowledges the fellowship provided by Setaram, Inc. for conducting the calorimetric research at WSU. Portions of

369 this research were also supported by collaboration, services, and infrastructure through the  
370 Nuclear Science Center User Facility at WSU and the WSU-PNNL Nuclear Science and  
371 Technology Institute.

## Tables

**Table 1** Thermochemical cycles used for calculations of the enthalpy of formation from binary oxides and the standard enthalpy of formation of stetindite based on the data of drop solution calorimetry in molten sodium molybdate saturated with amorphous silica at 25°C.

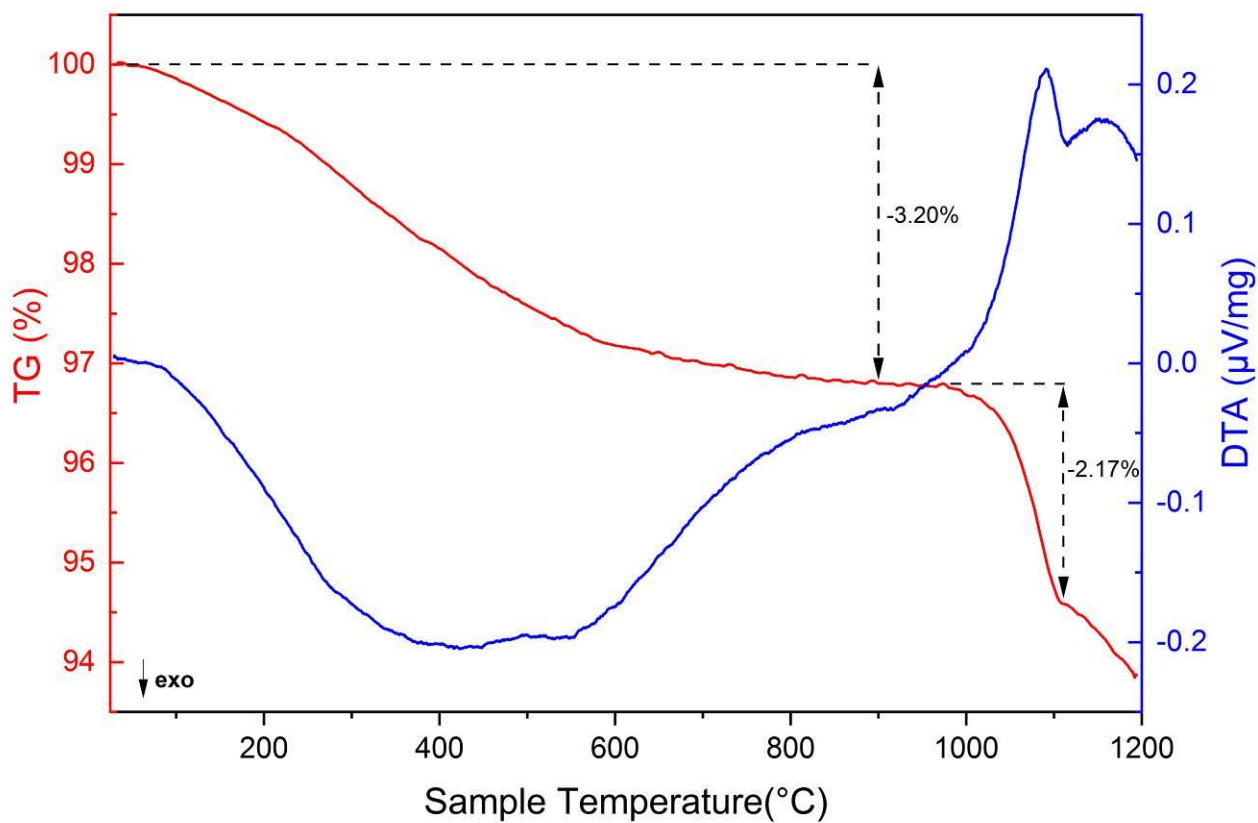
Reaction	$\Delta H$ (kJ/mol)
(1) $\text{CeSiO}_4 \cdot 0.43\text{H}_2\text{O}_{(\text{s}, 25^\circ\text{C})} \rightarrow \text{CeO}_{2(\text{sln}, 700^\circ\text{C})} + \text{SiO}_{2(\text{cristobalite}, 700^\circ\text{C})} + 0.43 \text{H}_2\text{O}_{(\text{g}, 700^\circ\text{C})}$	$\Delta H_1 = 95.36^* \pm 3.52^\dagger (3)^\ddagger$
(2) $\text{CeSiO}_4 (\text{s}, 25^\circ\text{C}) \rightarrow \text{CeO}_{2(\text{sln}, 700^\circ\text{C})} + \text{SiO}_{2(\text{cristobalite}, 700^\circ\text{C})}$	$\Delta H_2 = 92.88 \pm 3.40 (2)$
(3) $\text{CeO}_{2(\text{s}, 25^\circ\text{C})} \rightarrow \text{CeO}_{2(\text{sln}, 700^\circ\text{C})}$	$\Delta H_3 = 74.37 \pm 0.75^{58} (66)$
(4) $\text{SiO}_{2(\text{quartz}, 25^\circ\text{C})} \rightarrow \text{SiO}_{2(\text{cristobalite}, 700^\circ\text{C})}$	$\Delta H_4 = 43.54 \pm 0.60^{58} (3)$
(5) $\text{Ce}_{(\text{s}, 25^\circ\text{C})} + \text{O}_{2(\text{g}, 25^\circ\text{C})} \rightarrow \text{CeO}_{2(\text{s}, 25^\circ\text{C})}$	$\Delta H_5 = -1088.7 \pm 1.5^{117}$
(6) $\text{Si}_{(\text{s}, 25^\circ\text{C})} + \text{O}_{2(\text{g}, 25^\circ\text{C})} \rightarrow \text{SiO}_{2(\text{quartz}, 25^\circ\text{C})}$	$\Delta H_6 = -910.7 \pm 1.0^{117}$
(7) $\text{H}_2\text{O}_{(\text{l}, 25^\circ\text{C})} \rightarrow \text{H}_2\text{O}_{(\text{g}, 700^\circ\text{C})}$	$\Delta H_7 = 69.0^{117}$
(8) $\text{H}_2\text{O}_{(\text{l}, 25^\circ\text{C})} \rightarrow \text{H}_2\text{O}_{(\text{cr}, 25^\circ\text{C})}$	$\Delta H_8 = -80.0^{48}$
<b>Enthalpy of drop solution corrected for proper molar mass of the partially hydrated sample:</b>	
(9) $\text{CeSiO}_4 \cdot 0.025\text{H}_2\text{O}_{(\text{s}, 25^\circ\text{C})} \rightarrow \text{CeO}_{2(\text{sln}, 700^\circ\text{C})} + \text{SiO}_{2(\text{cristobalite}, 700^\circ\text{C})} + 0.025 \text{H}_2\text{O}_{(\text{g}, 700^\circ\text{C})}$	$\Delta H_9 = -92.48 \pm 3.42 (3)$
<b>Corrected enthalpy of drop solution value assuming water is strongly bonded:</b>	
(10) $\Delta H_{\text{ds}}(\text{CeSiO}_4) = \Delta H_{10} = \Delta H_9 - 0.025 \cdot (\Delta H_6 + \Delta H_7)$	$\Delta H_{\text{ds}} = 88.7 \pm 3.4$
<b>Enthalpy of formation of stetindite from <math>\text{CeO}_2</math> and <math>\text{SiO}_2</math> (quartz) assuming water is strongly bonded:</b>	
(11) $\Delta H_{\text{f,ox}}(\text{CeSiO}_4) = \Delta H_{11} = -\Delta H_{10} + \Delta H_3 + \Delta H_4$	$\Delta H_{\text{f,ox}} = 29.2 \pm 3.5$
<b>Standard enthalpy of formation of stetindite assuming water is strongly bonded</b>	
(12) $\Delta H^\circ_{\text{f}}(\text{CeSiO}_4) = \Delta H_{11} + \Delta H_4 + \Delta H_5$	$\Delta H^\circ_{\text{f}} = -1970.2 \pm 4.0$
<b>Enthalpy of formation of dehydrated stetindite from <math>\text{CeO}_2</math> and <math>\text{SiO}_2</math> (quartz):</b>	
(13) $\Delta H_{\text{f,ox}}(\text{CeSiO}_4) = \Delta H_{13} = -\Delta H_2 + \Delta H_3 + \Delta H_4$	$\Delta H_{\text{f,ox}} = 25.0 \pm 3.5$
<b>Standard enthalpy of formation of stetindite:</b>	
(14) $\Delta H^\circ_{\text{f}}(\text{CeSiO}_4) = \Delta H_{13} + \Delta H_4 + \Delta H_5$	$\Delta H^\circ_{\text{f}} = -1974.2 \pm 4.0$

\* Average. <sup>†</sup> Two standard deviations of the average value. <sup>‡</sup> Number of measurements.

**Table 2** Enthalpy of formation from oxides for orthosilicate end-members, coming from experiments and calculations at 25°C.

	<b>8 CN A<sup>4+</sup> Ionic Radii</b> (Å)	<b><math>\Delta H^\circ_f \text{AO}_2</math></b> (kJ/mol)	<b><math>\Delta H^\circ_f \text{ASiO}_4</math></b> (kJ/mol)	<b><math>\Delta H_{f, \text{ox}, 25^\circ\text{C}}</math></b> <b>ASiO<sub>4</sub> (kJ/mol)</b>
<b>zircon</b>	0.83	-1100.6 ± 1.7 <sup>a</sup>	-2035.5 ± 3.4 <sup>a</sup>	-24.2 ± 2.8 <sup>a</sup>
<b>hafnon</b>	0.84	-1117.6 ± 1.6 <sup>a</sup>	-2050.3 ± 5.1 <sup>a</sup>	-22.3 ± 4.7 <sup>a</sup>
<b>stetindite</b>	0.97	-1090.4 ± 1.0 <sup>b</sup>	-1971.9 ± 3.6 <sup>c</sup>	27.5 ± 3.1 <sup>c</sup>
<b>thorite</b>	1.05	-1226.4 ± 3.5 <sup>b</sup>	-2143.5 ± 6.8 <sup>c</sup>	-6.4 ± 5.7 <sup>c</sup>
<b>PaSiO<sub>4</sub></b>	1.01	-1107.0 ± 15.0 <sup>b</sup>	-2003.6 ± 15.1 <sup>f</sup>	14.1 ± 2.9 <sup>f</sup>
<b>coffinite</b>	1.00	-1085.0 ± 1.0 <sup>b</sup>	-1970.0 ± 4.2 <sup>d</sup>	25.6 ± 3.9 <sup>d</sup>
<b>NpSiO<sub>4</sub></b>	0.98	-1078.5 ± 2.7 <sup>b</sup>	-1961.7 ± 4.1 <sup>f</sup>	27.5 ± 5.7 <sup>f</sup>
<b>PuSiO<sub>4</sub></b>	0.96	-1055.8 ± 1.0 <sup>b</sup>	-1930.1 ± 4.1 <sup>f</sup>	36.4 ± 7.6 <sup>f</sup>
<b>AmSiO<sub>4</sub></b>	0.95	-932.2 ± 3.0 <sup>b</sup>	-1802.0 ± 5.3 <sup>f</sup>	40.9 ± 8.5 <sup>f</sup>
<b>CmSiO<sub>4</sub></b>	0.95	Not Available	Not Available	40.9 ± 8.5 <sup>f</sup>
<b>BkSiO<sub>4</sub></b>	0.93	Not Available	Not Available	49.8 ± 10.4 <sup>f</sup>
<b>CfSiO<sub>4</sub></b>	0.92	Not Available	Not Available	54.3 ± 11.3 <sup>f</sup>

<sup>a</sup>. Navrotsky and Ushakov (2005)<sup>118</sup>; <sup>b</sup>. Konings *et al.* (2014)<sup>105</sup>; <sup>c</sup>. Guo *et al.* (2016)<sup>8</sup>; <sup>d</sup>. Guo *et al.* (2015)<sup>48</sup>; <sup>e</sup>. Experimentally derived in this study; <sup>f</sup>. Calculated in this study.

383 **Figures**

384  
 385 **Figure 1.** TGA-DTA curve obtained from  $\text{CeSiO}_4 \cdot 0.43\text{H}_2\text{O}$  (sample mass:  $4.5220 \pm 0.0005$  mg)  
 386 when heating up to  $1200^\circ\text{C}$  under  $\text{N}_2$  atmosphere.

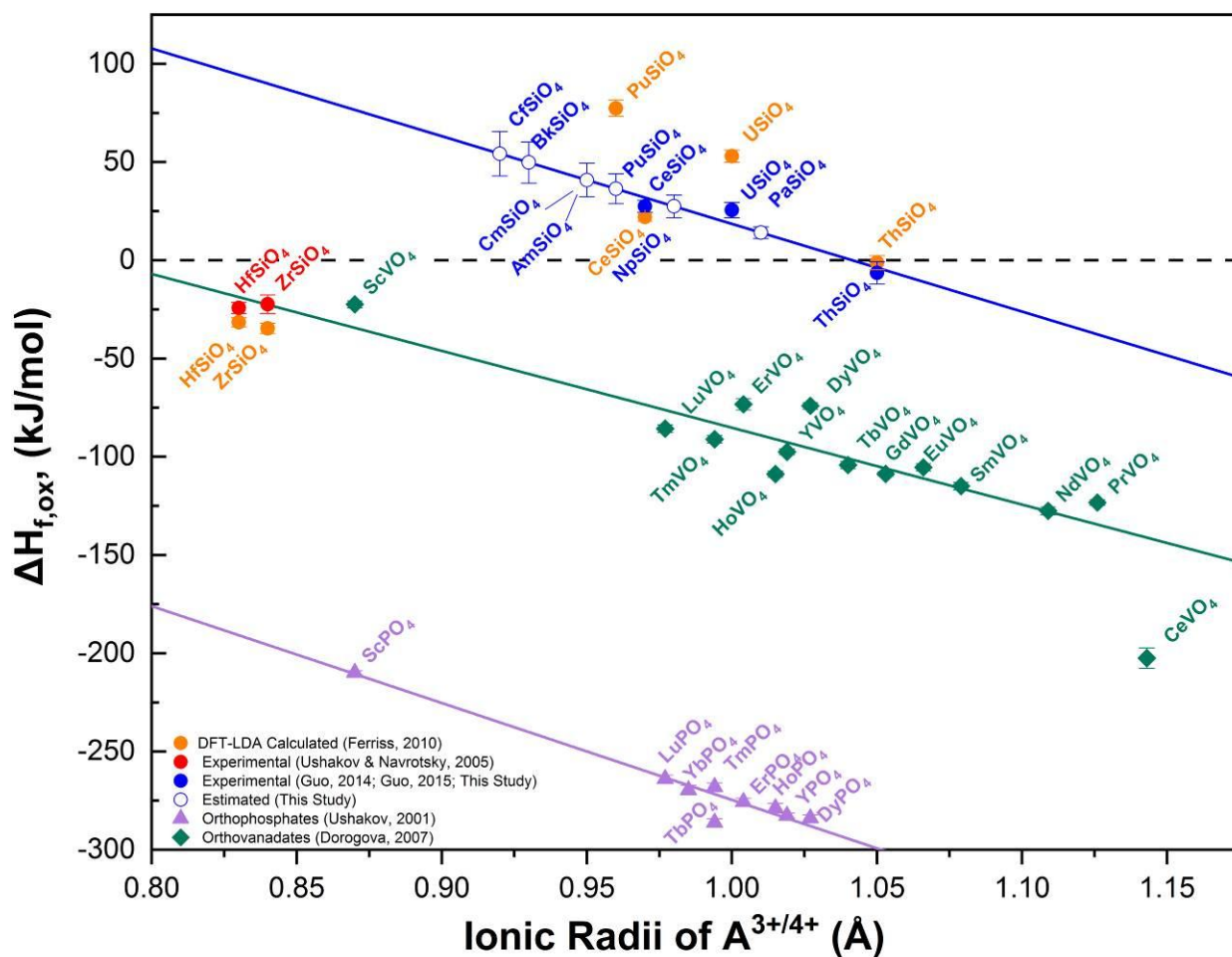


**Figure 2.** Enthalpy of formation from binary oxides obtained for orthosilicates ( $\text{ASiO}_4$ ), orthovanadates ( $\text{AVO}_4$ ), and orthophosphates ( $\text{APO}_4$ ) that crystallize with the zircon structure ( $I4_1/amd$ ) as a function of ionic radius of a metal cation ( $\text{A}^{4+}$  or  $\text{A}^{3+}$ ) in the eightfold coordination. Data shown as *filled blue circles* were used in order to estimate the values for the *empty blue circles* by means of linear regression. The equation which describes the *blue line* is  $\Delta H_{f, \text{ox}} = (-446.3 \pm 152.5) r - (464.9 \pm 153.6)$ , with an adjusted  $R^2 = 0.79096$ . Data denoted with *orange circles* was derived by utilizing the DFT-LDA results for the enthalpy of formation of orthosilicate materials at  $-273^\circ\text{C}$  reported by Ferriss *et al.*<sup>37</sup>, in conjunction with the standard enthalpy of formation of quartz<sup>117</sup> and  $\text{AO}_2$ <sup>105</sup> ( $\text{A} = \text{Ce}, \text{U}, \text{Th}, \text{Pu}$ ). This assumes that the energetic contributions from the respective heat capacities are negligible to the overall calculation, so the enthalpy of formation data reported by Ferriss *et al.* can be treated as approximately equal to standard state conditions. Data points as *purple triangles* and *green diamonds* are for orthophosphates<sup>59</sup> and orthovanadates<sup>106</sup>, respectively.

## References:

- (1) Burns, P. C.; Ewing, R. C.; Navrotsky, A. Nuclear Fuel in a Reactor Accident. *Science* (80-. ). **2012**, 335 (6073), 1184–1188. <https://doi.org/10.1126/science.1211285>.
- (2) Orlova, A. I.; Ojovan, M. I. Ceramic Mineral Waste-Forms for Nuclear Waste Immobilization. *Materials* (Basel). **2019**, 12 (16), 2638. <https://doi.org/10.3390/ma12162638>.
- (3) Goel, A.; McCloy, J. S.; Pokorny, R.; Kruger, A. A. Challenges with Vitrification of Hanford High-Level Waste (HLW) to Borosilicate Glass – *An Overview*. *J. Non-Crystalline Solids X*. **2019**, 4 (August), 1–19. <https://doi.org/10.1016/j.nocx.2019.100033>.
- (4) Wegel, S.; Czempinski, V.; Oei, P.-Y.; Wealer, B. Transporting and Storing High-Level Nuclear Waste in the U.S.-Insights from a Mathematical Model. *Appl. Sci*. **2019**, 9 (12). <https://doi.org/10.3390/app9122437>.
- (5) Weber, W. J.; Navrotsky, A.; Stefanovsky, S.; Vance, E. R.; Vernaz, E. Materials Science of High-Level Immobilization. *MRS Bull.* **2009**, 34 (January 2009). <https://doi.org/https://doi.org/10.1557/mrs2009.12>.
- (6) Ewing, R. C. Long-Term Storage of Spent Nuclear Fuel. *Nat. Mater.* **2015**, 14 (3), 252–257. <https://doi.org/10.1038/nmat4226>.
- (7) Guo, X.; Navrotsky, A.; Kukkadapu, R. K.; Engelhard, M. H.; Lanzirrotti, A.; Newville, M.; Ilton, E. S.; Sutton, S. R.; Xu, H. Structure and Thermodynamics of Uranium-Containing Iron Garnets. *Geochim. Cosmochim. Acta*. **2016**, 189, 269–281. <https://doi.org/10.1016/j.gca.2016.05.043>.
- (8) Guo, X.; Szenknect, S.; Mesbah, A.; Clavier, N.; Poinssot, C.; Wu, D.; Xu, H.; Dacheux, N.; Ewing, R. C.; Navrotsky, A. Energetics of a Uranothorite ( $\text{Th}_{1-x}\text{U}_x\text{SiO}_4$ ) Solid Solution. *Chem. Mater.* **2016**, 28 (19), 7117–7124. <https://doi.org/10.1021/acs.chemmater.6b03346>.
- (9) Guo, X.; Tavakoli, A. H.; Sutton, S.; Kukkadapu, R. K.; Qi, L.; Lanzirrotti, A.; Newville, M.; Asta, M.; Navrotsky, A. Cerium Substitution in Yttrium Iron Garnet: Valence State, Structure, and Energetics. *Chem. Mater.* **2014**, 26 (2), 1133–1143. <https://doi.org/10.1021/cm403444f>.
- (10) Chung, C. K.; O’Quinn, E. C.; Neuefeind, J. C.; Fuentes, A. F.; Xu, H.; Lang, M.; Navrotsky, A. Thermodynamic and Structural Evolution of Mechanically Milled and Swift Heavy Ion Irradiated  $\text{Er}_2\text{Ti}_2\text{O}_7$  Pyrochlore. *Acta Mater.* **2019**, 181, 309–317. <https://doi.org/10.1016/j.actamat.2019.09.022>.
- (11) Helean, K. B.; Navrotsky, A.; Vance, E. R.; Carter, M. L.; Ebbinghaus, B.; Krikorian, O.; Lian, J.; Wang, L. M.; Catalano, J. G. Enthalpies of Formation of Ce-Pyrochlore,  $\text{Ca}_{0.93}\text{Ce}_{1.00}\text{Ti}_{2.035}\text{O}_{7.00}$ , U-Pyrochlore,  $\text{Ca}_{1.46}\text{U}^{4+}_{0.23}\text{U}^{6+}_{0.46}\text{Ti}_{1.85}\text{O}_{7.00}$  and Gd-Pyrochlore,  $\text{Gd}_2\text{Ti}_2\text{O}_7$ : Three Materials Relevant to the Proposed Waste Form for Excess Weapons Plutonium. *J. Nucl. Mater.* **2002**, 303 (2–3), 226–239. [https://doi.org/10.1016/s0022-3115\(02\)00795-x](https://doi.org/10.1016/s0022-3115(02)00795-x).
- (12) Neumeier, S.; Kegler, P.; Arinicheva, Y.; Shelyug, A.; Kowalski, P. M.; Schreinemachers, C.; Navrotsky, A.; Bosbach, D. Thermochemistry of  $\text{La}_{1-x}\text{Ln}_x\text{PO}_4$ -Monazites (Ln = Gd, Eu). *J. Chem. Thermodyn.* **2017**, 105, 396–403. <https://doi.org/10.1016/j.jct.2016.11.003>.
- (13) Ewing, R. C.; Lutze, W.; Weber, W. J. Zircon: A Host-Phase for the Disposal of Weapons Plutonium. *J. Mater. Res.* **1995**, 10 (2), 243–246. <https://doi.org/10.1557/JMR.1995.0243>.
- (14) Ewing, R. C. Nuclear Waste Forms for Actinides. *Proc. Natl. Acad. Sci. U. S. A.* **1999**, 96 (7), 3432–3439. <https://doi.org/10.1073/pnas.96.7.3432>.
- (15) Ushakov, S. V.; Gong, W.; Yagokina, M. M.; Helean, K. B.; Lutze, W.; Ewing, R. C. Solid Solutions of Ce, U, and Th in Zircon. *Ceram. Trans.* **1999**, 93, 357–363.
- (16) White, W. M. Isotope Geochemistry, 1st ed.; John Wiley & Sons, **2015**.
- (17) Finch, R. J.; Hanchar, J. M. Structure and Chemistry of Zircon and Zircon-Group Minerals. *Rev. Mineral. Geochemistry* **2003**, 53 (1), 1–26.

- 449 (18) McCarthy, G. J.; White, W. B.; Pfoertsch, D. E. Synthesis of Nuclear Waste Monazites, Ideal  
450 Actinide Hosts for Geologic Disposal. *Mater. Res. Bull.* **1978**, 13 (11), 1239–1245.  
451 [https://doi.org/10.1016/0025-5408\(78\)90215-5](https://doi.org/10.1016/0025-5408(78)90215-5).
- 452 (19) Ewing, R. C. The Design and Evaluation of Nuclear-Waste Forms: Clues from Mineralogy.  
453 *Can. Mineral.* **2001**, 39 (3), 697–715. <https://doi.org/10.2113/gscanmin.39.3.697>.
- 454 (20) Lutze, W.; Ewing, R. C. Radioactive Waste Forms for the Future; North-Holland Physics  
455 Publishing: Amsterdam, **1988**.
- 456 (21) Ewing, R. C.; Weber, W. J. Actinide Waste Forms and Radiation Effects. In The Chemistry  
457 of the Actinide and Transactinide Elements; Morss, L. R., Edelstein, N. M., Fuger, J., Eds.;  
458 Springer: Dordrecht, **2010**; Vol. 3813, pp 3813–3887. [https://doi.org/10.1007/978-94-007-0211-](https://doi.org/10.1007/978-94-007-0211-0_35)  
459 [0\\_35](https://doi.org/10.1007/978-94-007-0211-0_35).
- 460 (22) Weber, W. J.; Ewing, R. C. Chapter 10: Ceramic Waste Forms for Uranium and  
461 Transuranium Elements. In Uranium: Cradle to Grave; Burns, P. C., Sigmon, G. E., Eds.;  
462 Mineralogical Association of Canada, **2013**; pp 317–336.
- 463 (23) Weber, W. J.; Ewing, R. C.; Vance, E. R.; Gregg, D.; Peugeot, S.; Wiss, T. Plutonium in  
464 Waste Forms. In Plutonium Handbook; Clark, D. L., Geeson, D. A., Hanrahan Jr., R. J., Eds.;  
465 American Nuclear Society, **2019**; pp 2349–2422.
- 466 (24) Ewing, R. C.; Weber, W. J.; Clinard, F. W. Radiation Effects in Nuclear Waste Forms for  
467 High-Level Radioactive Waste. *Prog. Nucl. Energy* **1995**, 29 (2), 63–127.  
468 [https://doi.org/10.1016/0149-1970\(94\)00016-Y](https://doi.org/10.1016/0149-1970(94)00016-Y).
- 469 (25) Weber, W. J.; Ewing, R. C.; Lutze, W. Performance Assessment of Zircon as a Waste Form  
470 for Excess Weapons Plutonium Under Deep Borehole Burial Conditions. *Mater. Res. Soc. Symp. -*  
471 *Proc.* **1996**, 412, 25–32. <https://doi.org/https://doi.org/10.1557/PROC-412-25>.
- 472 (26) McMurdie, H. F.; Hall, F. P. Phase Diagrams for Ceramists: Supplement No. 1. *J. Am.*  
473 *Ceram. Society.* **1947**, No. 1, 154–164.
- 474 (27) Grover, V.; Tyagi, A. K. Preparation and Bulk Thermal Expansion Studies in  $M_{1-x}Ce_xSiO_4$   
475 ( $M = Th, Zr$ ) System, and Stabilization of Tetragonal  $ThSiO_4$ . *J. Alloys Comps.* **2005**, 390 (1–2),  
476 112–114. <https://doi.org/10.1016/j.jallcom.2004.05.091>.
- 477 (28) Subbarao, E. C.; Agrawal, D. K.; McKinstry, H. A.; Sallese, C. W.; Roy, R. Thermal  
478 Expansion of Compounds of Zircon Structure. *J. Am. Ceram. Soc.* **1990**, 73 (5), 1246–1252.  
479 <https://doi.org/10.1111/j.1151-2916.1990.tb05187.x>.
- 480 (29) Nesse, W. D. Introduction to Mineralogy, 2nd ed.; Oxford University Press, **2000**.
- 481 (30) Poirrot, I. S.; Kot, W. K.; Edelstein, N. M.; Abraham, M. M.; Finch, C. B.; Boatner, L. A.  
482 Optical Study and Analysis of  $Pu^{4+}$  in Single Crystals of  $ZrSiO_4$ . *Phys. Rev. B* **1989**, 39 (10),  
483 6388–6394. <https://doi.org/10.1103/PhysRevB.39.6388>.
- 484 (31) Weber, W. J. Radiation-Induced Defects and Amorphization in Zircon. *J. Mater. Res.* **1990**, 5  
485 (11), 2687–2697. <https://doi.org/10.1557/JMR.1990.2687>.
- 486 (32) Weber, W. J. Alpha-Decay-Induced Amorphization in Complex Silicate Structures. *J. Am.*  
487 *Ceram. Soc.* **1993**, 76 (7), 1729–1738. <https://doi.org/10.1111/j.1151-2916.1993.tb06641.x>.
- 488 (33) Anderson, E. B.; Burakov, B. E.; Pazukhin, E. M. High-Uranium Zircon from “Chernobyl  
489 Lavas.” *Radiochim. Acta* **1992**, 60 (2–3), 149–152. <https://doi.org/10.1524/ract.1993.60.23.149>.
- 490 (34) Keller, V. C. Untersuchungen Über Die Germanate Und Silikate Des Typs  $ABO_4$  Der  
491 Vierwertigen Elemente Thorium Bis Americium. *Nukleonik* **1963**, No. 5, 41–48.
- 492 (35) Estevenon, P.; Welcomme, E.; Tamain, C.; Jouan, G.; Szenknect, S.; Mesbah, A.; Poinssot,  
493 C.; Moisy, P.; Dacheux, N. Formation of  $PuSiO_4$  under Hydrothermal Conditions. *Dalt. Trans.*  
494 **2020**. <https://doi.org/https://doi.org/10.1039/D0DT01183E>.

- (36) Hanchar, J. M.; Burakov, B. E.; Zamoryanskaya, M. V.; Garbuzov, V. M.; Kitsay, A. A.; Zirlin, V. A. Investigation of Pu Incorporation into Zircon Single Crystal. *Mater. Res. Soc. Symp. Proc.* **2004**, 824, 225–229. <https://doi.org/10.1557/proc-824-cc4.2>.
- (37) Ferriss, E. D. A.; Ewing, R. C.; Becker, U. Simulation of Thermodynamic Mixing Properties of Actinide-Containing Zircon Solid Solutions. *Am. Mineral.* **2010**, 95 (2–3), 229–241. <https://doi.org/10.2138/am.2010.3318>.
- (38) Zamoryanskaya, M. V.; Burakov, B. E. Feasibility Limits in Using Cerium as a Surrogate for Plutonium Incorporation in Zircon, Zirconia and Pyrochlore. *Mater. Res. Soc. Symp. - Proc.* **2001**, 663, 301–306. <https://doi.org/10.1557/proc-663-301>.
- (39) Putnam, R. L.; Navrotsky, A.; Cordfunke, E. H. P.; Huntelaar, M. E. Thermodynamics of Formation of Two Cerium Aluminum Oxides,  $\text{CeAlO}_{3(s)}$  And  $\text{CeAl}_{12}\text{O}_{19.918(s)}$ , and Cerium Sesquioxide,  $\text{Ce}_2\text{O}_{3(s)}$  At  $T = 298.15$  K. *J. Chem. Thermodyn.* **2000**, 32 (7), 911–921. <https://doi.org/10.1006/jcht.2000.0665>.
- (40) Putnam, R. L.; Gallegos, U. F.; Ebbinghaus, B. B.; Navrotsky, A.; Helean, K. B.; Ushakov, S. V.; Woodfield, B. F.; Boerio-Goates, J.; Williamson, M. A. Formation Energetics of Ceramic Phases Related to Surplus Plutonium Disposition. *Ceram. Trans.* **2001**, 119(Enviro), 147–158.
- (41) Marra, J. C.; Cozzi, A. D.; Pierce, R. A.; Pareizs, J. M.; Jurgensen, A. R.; Missimer, D. M. Cerium as a Surrogate in the Plutonium Immobilized Form. In Environmental Issues and Waste Management Technologies in the Ceramic and Nuclear Industries; Smith, G. L., Sundaram, S. K., Spearing, D. R., Eds.; *American Ceramic Society*, **2002**; pp 381–388.
- (42) Shannon, R. D. Revised Effective Ionic Radii and Systematic Studies of Interatomic Distances in Halides and Chalcogenides. *Acta Crystallogr. Sect. A* **1976**, 32 (5), 751–766. <https://doi.org/10.1107/S0567739476001563>.
- (43) Estevenon, P.; Welcomme, E.; Szenknect, S.; Mesbah, A.; Moisy, P.; Poinssot, C.; Dacheux, N. Preparation of  $\text{CeSiO}_4$  from Aqueous Precursors under Soft Hydrothermal Conditions. *Dalt. Trans.* **2019**, 48 (22), 7551–7559. <https://doi.org/10.1039/c9dt01258c>.
- (44) Estevenon, P.; Kaczmarek, T.; Vadot, F.; Dumas, T.; Solari, P. L.; Welcomme, E.; Szenknect, S.; Mesbah, A.; Moisy, P.; Poinssot, C.; Dacheux, N. Formation of  $\text{CeSiO}_4$  from Cerium (III) Silicate Precursors. *Dalt. Trans.* **2019**, 48, 10455–10463. <https://doi.org/10.1039/c9dt01990a>.
- (45) Sverjensky, D. A.; Molling, P. A. A Linear Free Energy Relationship for Crystalline Solids and Aqueous Ions. *Nature* **1992**, 356 (6366), 231–234. <https://doi.org/10.1038/356231a0>.
- (46) Navrotsky, A. Systematic Trends and Prediction of Enthalpies of Formation of Refractory Lanthanide and Actinide Ternary Oxide Phases. *Ceram. Trans.* **2001**, No. 119, 137–146.
- (47) Helean, K. B.; Navrotsky, A.; Lumpkin, G. R.; Colella, M.; Lian, J.; Ewing, R. C.; Ebbinghaus, B.; Catalano, J. G. Enthalpies of Formation of U-, Th-, Ce-Brannerite: Implications for Plutonium Immobilization. *J. Nucl. Mater.* **2003**, 320 (3), 231–244. [https://doi.org/10.1016/S0022-3115\(03\)00186-7](https://doi.org/10.1016/S0022-3115(03)00186-7).
- (48) Guo, X.; Szenknect, S.; Mesbah, A.; Labs, S.; Clavier, N.; Poinssot, C.; Ushakov, S. V.; Curtius, H.; Bosbach, D.; Ewing, R. C.; Burns, P.C.; Dacheux, N.; Navrotsky, A. Thermodynamics of Formation of Coffinite,  $\text{USiO}_4$ . *Proc. Natl. Acad. Sci.* **2015**, 112 (21), 6551–6555. <https://doi.org/10.1073/pnas.1507441112>.
- (49) Szenknect, S.; Mesbah, A.; Cordara, T.; Clavier, N.; Brau, H. P.; Le Goff, X.; Poinssot, C.; Ewing, R. C.; Dacheux, N. First Experimental Determination of the Solubility Constant of Coffinite. *Geochim. Cosmochim. Acta* **2016**, 181, 36–53. <https://doi.org/10.1016/j.gca.2016.02.010>.

- 541 (50) Costin, D. T.; Mesbah, A.; Clavier, N.; Dacheux, N.; Poinssot, C.; Szenknect, S.; Ravaux, J.  
542 How to Explain the Difficulties in the Coffinite Synthesis from the Study of Uranothorite? *Inorg.*  
543 *Chem.* **2011**, 50 (21), 11117–11126. <https://doi.org/10.1021/ic2016758>.
- 544 (51) Frondel, C.; Collette, R. L. Hydrothermal Synthesis of Zircon, Thorite and Huttonite. *Am.*  
545 *Mineral.* **1957**, 42 (378), 759–765.
- 546 (52) Mumpton, F. A.; Roy, R. Hydrothermal Stability Studies of the Zircon-Thorite Group.  
547 *Geochim. Cosmochim. Acta* **1961**, 21 (3–4), 217–238. [https://doi.org/10.1016/s0016-](https://doi.org/10.1016/s0016-7037(61)80056-2)  
548 [7037\(61\)80056-2](https://doi.org/10.1016/s0016-7037(61)80056-2).
- 549 (53) Estevenon, P.; Welcomme, E.; Szenknect, S.; Mesbah, A.; Moisy, P.; Poinssot, C.; Dacheux,  
550 N. Impact of Carbonate Ions on the Synthesis of ThSiO<sub>4</sub> under Hydrothermal Conditions. *Inorg.*  
551 *Chem.* **2018**, 57 (19), 12398–12408. <https://doi.org/10.1021/acs.inorgchem.8b02146>.
- 552 (54) Estevenon, P.; Welcomme, E.; Szenknect, S.; Mesbah, A.; Moisy, P.; Poinssot, C.; Dacheux,  
553 N. Multiparametric Study of the Synthesis of ThSiO<sub>4</sub> under Hydrothermal Conditions. *Inorg.*  
554 *Chem.* **2018**, 57 (15), 9393–9402. <https://doi.org/10.1021/acs.inorgchem.8b01390>.
- 555 (55) Schlüter, J.; Malcherek, T.; Husdal, T. A. The New Mineral Stetindite, CeSiO<sub>4</sub>, a Cerium  
556 End-Member of the Zircon Group. *Neues Jahrb. für Mineral. Abhandlungen* **2009**, 186 (2), 195–  
557 200. <https://doi.org/10.1127/0077-7757/2009/0146>.
- 558 (56) Navrotsky, A.; Kleppa, O. J. A Calorimetric Study of Molten Na<sub>2</sub>MoO<sub>4</sub>-MoO<sub>3</sub> Mixtures at  
559 970 K. *Inorg. Chem.* **1967**, 6 (11), 2119–2121. <https://doi.org/10.1021/ic50057a047>.
- 560 (57) Navrotsky, A. Progress and New Directions in High Temperature Calorimetry. *Phys. Chem.*  
561 *Miner.* 1977, 2 (December), 89–104.
- 562 (58) Navrotsky, A. Progress and New Directions in Calorimetry: A 2014 Perspective. *J. Am.*  
563 *Ceram. Soc.* 2014, 97 (11), 3349–3359. <https://doi.org/10.1111/jace.13278>.
- 564 (59) Ushakov, S. V.; Helean, K. B.; Navrotsky, A.; Boatner, L. A. Thermochemistry of Rare-Earth  
565 Orthophosphates. *J. Mater. Res.* **2001**, 16 (9), 2623–2633.  
566 <https://doi.org/10.1557/JMR.2001.0361>.
- 567 (60) Helean, K. B.; Navrotsky, A. Oxide Melt Solution Calorimetry of Rare Earth Oxides.  
568 Techniques, Problems, Cross-Checks, Successes. *J. Therm. Anal. Calorim.* **2002**, 69 (3), 751–771.  
569 <https://doi.org/10.1023/A:1020687418374>.
- 570 (61) Guo, X.; Boukhalfa, H.; Mitchell, J. N.; Ramos, M.; Gaunt, A. J.; Migliori, A.; Roback, R.  
571 C.; Navrotsky, A.; Xu, H. Sample Seal-and-Drop Device and Methodology for High Temperature  
572 Oxide Melt Solution Calorimetric Measurements of PuO<sub>2</sub>. *Rev. Sci. Instrum.* **2019**, 90 (4),  
573 044101. <https://doi.org/10.1063/1.5093567>
- 574 (62) Gorman-Lewis, D.; Mazeina, L.; Fein, J. B.; Szymanowski, J. E. S.; Burns, P. C.; Navrotsky,  
575 A. Thermodynamic Properties of Soddyite from Solubility and Calorimetry Measurements. *J.*  
576 *Chem. Thermodyn.* **2007**, 39 (4), 568–575. <https://doi.org/10.1016/j.jct.2006.09.005>.
- 577 (63) Navrotsky, A.; Shvareva, T.; Guo, X. Thermodynamics of Uranium Minerals and Related  
578 Materials. In Mineralogical Association of Canada Short Course 43; **2013**; pp 1–18.
- 579 (64) Guo, X.; Tiferet, E.; Qi, L.; Solomon, J. M.; Lanzirotti, A.; Newville, M.; Engelhard, M. H.;  
580 Kukkadapu, R. K.; Wu, D.; Ilton, E. S.; Asta, M.; Sutton, S.R.; Xu, H.; Navrotsky, A. U(v) in  
581 Metal Uranates: A Combined Experimental and Theoretical Study of MgUO<sub>4</sub>, CrUO<sub>4</sub>, and FeUO<sub>4</sub>.  
582 *Dalt. Trans.* **2016**, 45 (11), 4622–4632. <https://doi.org/10.1039/c6dt00066e>.
- 583 (65) Guo, X.; Wu, D.; Xu, H.; Burns, P. C.; Navrotsky, A. Thermodynamic Studies of Studtite  
584 Thermal Decomposition Pathways via Amorphous Intermediates UO<sub>3</sub>, U<sub>2</sub>O<sub>7</sub>, and UO<sub>4</sub>. *J. Nucl.*  
585 *Mater.* **2016**, 478, 158–163. <https://doi.org/10.1016/j.jnucmat.2016.06.014>.
- 586 (66) Clavier, N.; Szenknect, S.; Costin, D. T.; Mesbah, A.; Poinssot, C.; Dacheux, N. From  
587 Thorite to Coffinite: A Spectroscopic Study of Th<sub>1-x</sub>U<sub>x</sub>SiO<sub>4</sub> Solid Solutions. *Spectrochim. Acta -*  
588 *Part A Mol. Biomol. Spectrosc.* **2014**, 118, 302–307. <https://doi.org/10.1016/j.saa.2013.08.093>.

- 589 (67) Speer, J. A.; Cooper, B. J. Crystal Structure of Synthetic Hafnon,  $\text{HfSiO}_4$ , Comparison with  
590 Zircon and the Actinide Orthosilicates. *Am. Mineral.* **1982**, 67 (7–8), 804–808.
- 591 (68) Janeczek, J.; Ewing, R. C. Coffinitization - A Mechanism for the Alteration of  $\text{UO}_2$  under  
592 Reducing Conditions. *Mater. Res. Soc. Symp. Proc.* **1992**, 257.  
593 <https://doi.org/10.1017/CBO9781107415324.004>.
- 594 (69) Finch, R.; Murakami, T. Systematics and Paragenesis of Uranium Minerals. In Uranium:  
595 Mineralogy, Geochemistry, and the Environment; Burns, P. C., Finch, R. J., Eds.; **1999**; pp 91–  
596 179. <https://doi.org/10.1515/9781501509193-008>.
- 597 (70) Janeczek, J. Composition and Origin of Coffinite from Jachymov, Czechoslovakia. *Neues*  
598 *Jahrb. für Mineral. Monatshefte* **1991**, 9, 385–395.
- 599 (71) Nasdala, L.; Beran, A.; Libowitzky, E.; Wolf, D. The Incorporation of Hydroxyl Groups and  
600 Molecular Water in Natural Zircon ( $\text{ZrSiO}_4$ ). *Am. J. Sci.* **2001**, 301 (10), 831–857.  
601 <https://doi.org/10.2475/ajs.301.10.831>.
- 602 (72) Miller, F. A.; Wilkins, C. H. Infrared Spectra and Characteristic Frequencies of Inorganic  
603 Ions. *Anal. Chem.* **1952**, 24 (8), 1253–1294. <https://doi.org/10.1021/ac60068a007>.
- 604 (73) Speer, J. A. Zircon. In Reviews in Mineralogy and Geochemistry; **1982**; Vol. 5, pp 66–112.
- 605 (74) Labs, S.; Hennig, C.; Weiss, S.; Curtius, H.; Zänker, H.; Bosbach, D. Synthesis of Coffinite,  
606  $\text{USiO}_4$ , and Structural Investigations of  $\text{U}_x\text{Th}_{(1-x)}\text{SiO}_4$  Solid Solutions. *Environ. Sci. Technol.*  
607 **2014**, 48 (1), 854–860. <https://doi.org/10.1021/es403995b>.
- 608 (75) Hirono, T.; Tanikawa, W. Implications of the Thermal Properties and Kinetic Parameters of  
609 Dehydroxylation of Mica Minerals for Fault Weakening, Frictional Heating, and Earthquake  
610 Energetics. *Earth Planet. Sci. Lett.* **2011**, 307 (1–2), 161–172.  
611 <https://doi.org/10.1016/j.epsl.2011.04.042>.
- 612 (76) Perrillat, J. P.; Daniel, I.; Koga, K. T.; Reynard, B.; Cardon, H.; Crichton, W. A. Kinetics of  
613 Antigorite Dehydration: A Real-Time X-Ray Diffraction Study. *Earth Planet. Sci. Lett.* **2005**, 236  
614 (3–4), 899–913. <https://doi.org/10.1016/j.epsl.2005.06.006>.
- 615 (77) Tavakoli, A. H.; Maram, P. S.; Widgeon, S. J.; Rufner, J.; Van Benthem, K.; Ushakov, S.;  
616 Sen, S.; Navrotsky, A. Amorphous Alumina Nanoparticles: Structure, Surface Energy, and  
617 Thermodynamic Phase Stability. *J. Phys. Chem. C* **2013**, 117 (33), 17123–17130.  
618 <https://doi.org/10.1021/jp405820g>.
- 619 (78) Levchenko, A. A.; Li, G.; Boerio-Goates, J.; Woodfield, B. F.; Navrotsky, A.  $\text{TiO}_2$  Stability  
620 Landscape: Polymorphism, Surface Energy, and Bound Water Energetics. *Chem. Mater.* **2006**, 18  
621 (26), 6324–6332. <https://doi.org/10.1021/cm061183c>.
- 622 (79) Ushakov, S. V.; Navrotsky, A. Direct Measurements of Water Adsorption Enthalpy on  
623 Hafnia and Zirconia. *Appl. Phys. Lett.* **2005**, 87 (16), 1–3. <https://doi.org/10.1063/1.2108113>.
- 624 (80) Chen, F.; Ewing, R. C.; Clark, S. B. The Gibbs Free Energies and Enthalpies of Formation of  
625  $\text{U}^{6+}$  Phases: An Empirical Method of Prediction. *Am. Mineral.* **1999**, 84 (4), 650–664.  
626 <https://doi.org/10.2138/am-1999-0418>.
- 627 (81) Xu, H.; Wang, Y.; Barton, L. L. Application of a Linear Free Energy Relationship to  
628 Crystalline Solids of  $\text{MO}_2$  and  $\text{M}(\text{OH})_4$ . *J. Nucl. Mater.* **1999**, 273 (3), 343–346.  
629 [https://doi.org/10.1016/S0022-3115\(99\)00092-6](https://doi.org/10.1016/S0022-3115(99)00092-6).
- 630 (82) Xu, H.; Wang, Y. Use of Linear Free Energy Relationship to Predict Gibbs Free Energies of  
631 Formation of Pyrochlore Phases ( $\text{CaMTi}_2\text{O}_7$ ). *J. Nucl. Mater.* **1999**, 275 (2), 216–220.  
632 [https://doi.org/10.1016/S0022-3115\(99\)00189-0](https://doi.org/10.1016/S0022-3115(99)00189-0).
- 633 (83) Navrotsky, A. Thermochemical Insights into Refractory Ceramic Materials Based on Oxides  
634 with Large Tetravalent Cations. *J. Mater. Chem.* **2005**, 15 (19), 1883–1890.  
635 <https://doi.org/10.1039/b417143h>.

- (84) Qi, J.; Guo, X.; Mielewczyk-Gryn, A.; Navrotsky, A. Formation Enthalpies of  $\text{LaLnO}_3$  (Ln=Ho, Er, Tm and Yb) Interlanthanide Perovskites. *J. Solid State Chem.* **2015**, 227, 150–154. <https://doi.org/10.1016/j.jssc.2015.03.026>.
- (85) Helean, K. B.; Ushakov, S. V.; Brown, C. E.; Navrotsky, A.; Lian, J.; Ewing, R. C.; Farmer, J. M.; Boatner, L. A. Formation Enthalpies of Rare Earth Titanate Pyrochlores. *J. Solid State Chem.* **2004**, 177 (6), 1858–1866. <https://doi.org/10.1016/j.jssc.2004.01.009>.
- (86) Cotton, S. Lanthanide and Actinide Chemistry; John Wiley & Sons, Ltd, **2006**.
- (87) Seaborg, G. T. The Transuranium Elements. *Nature* **1946**, 104 (2704), 379–386. <https://doi.org/10.1038/159863a0>.
- (88) Seaborg, G. T. Origin of the Actinide Concept. In Handbook on the Physics and Chemistry of Rare Earths; Gschneidner, K. A., Eyring, L. J., Choppin, G. R., Lander, G. H., Eds.; Elsevier B.V, **1994**; Vol. 18, pp 1–26. [https://doi.org/https://doi.org/10.1016/S0168-1273\(05\)80041-8](https://doi.org/https://doi.org/10.1016/S0168-1273(05)80041-8).
- (89) Silver, M. A.; Albrecht-Schmitt, T. E. Evaluation of F-Element Borate Chemistry. *Coord. Chem. Rev.* **2016**, 323, 36–51. <https://doi.org/10.1016/j.ccr.2016.02.015>.
- (90) Albrecht-Schmitt, T. E. Organometallic and Coordination Chemistry of the Actinides; Springer, **2012**. <https://doi.org/10.1093/ntr/nts065>.
- (91) Horne, G. P.; Grimes, T. S.; Bauer, W. F.; Dares, C. J.; Pimblott, S. M.; Mezyk, S. P.; Mincher, B. J. Effect of Ionizing Radiation on the Redox Chemistry of Penta- And Hexavalent Americium. *Inorg. Chem.* **2019**, 58 (13), 8551–8559. <https://doi.org/10.1021/acs.inorgchem.9b00854>.
- (92) Sullivan, J. C.; Gordon, S.; Mulac, W. A.; Schmidt, K. H.; Cohen, D.; Sjoblom, R. Pulse Radiolysis Studies of Americium(III) and Curium(III) Ions in Perchlorate Media. The Preparation of Am II, Am IV, Cm II and Cm IV. *Inorg. Nucl. Chem. Lett.* **1976**, 12 (8), 599–601.
- (93) Keenan, T. K. Americium and Curium. *J. Chem. Educ.* 1959, 36 (1), 27–31. [https://doi.org/10.1142/9781860943096\\_0004](https://doi.org/10.1142/9781860943096_0004).
- (94) White, F. D.; Dan, D.; Albrecht-Schmitt, T. E. Contemporary Chemistry of Berkelium and Californium. *Chem. - A Eur. J.* **2019**, 25 (44), 10251–10261. <https://doi.org/10.1002/chem.201900586>.
- (95) Mincher, B. J.; Martin, L. R.; Schmitt, N. C. Diamylamylphosphonate Solvent Extraction of Am(VI) from Nuclear Fuel Raffinate Simulant Solution. *Solvent Extr. Ion Exch.* **2012**, 30 (5), 445–456. <https://doi.org/10.1080/07366299.2012.671108>.
- (96) Keenan, T. K. First Observation of Aqueous Tetravalent Curium. *J. Am. Chem. Soc.* **1961**, 83 (17), 3719–3720. <https://doi.org/10.1021/ja01478a039>.
- (97) Guo, X.; Xu, H. Enthalpies of Formation of Polyhalite: A Mineral Relevant to Salt Repository. *J. Chem. Thermodyn.* **2017**, 114, 44–47. <https://doi.org/10.1016/j.jct.2017.05.031>.
- (98) Xu, H.; Guo, X.; Bai, J. Thermal Behavior of Polyhalite: A High-Temperature Synchrotron XRD Study. *Phys. Chem. Miner.* **2017**, 44 (2), 125–135. <https://doi.org/10.1007/s00269-016-0842-5>.
- (99) Timofeev, A.; Migdisov, A. A.; Williams-Jones, A. E.; Roback, R.; Nelson, A. T.; Xu, H. Uranium Transport in Acidic Brines under Reducing Conditions. *Nat. Commun.* **2018**, 9 (1), 2–8. <https://doi.org/10.1038/s41467-018-03564-7>.
- (100) Fox, P. M.; Tinnacher, R. M.; Cheshire, M. C.; Caporuscio, F.; Carrero, S.; Nico, P. S. Effects of Bentonite Heating on U(VI) Adsorption. *Appl. Geochemistry* **2019**, 109 (July). <https://doi.org/10.1016/j.apgeochem.2019.104392>.
- (101) Utsunomiya, S.; Kersting, A. B.; Ewing, R. C. Groundwater Nanoparticles in the Far-Field at the Nevada Test Site: Mechanism for Radionuclide Transport. *Environ. Sci. Technol.* **2009**, 43 (5), 1293–1298. <https://doi.org/10.1021/es802181t>.

- 683 (102) Novikov, A. P.; Kalmykov, S. N.; Utsunomiya, S.; Ewing, R. C.; Horreard, F.; Merkulov,  
684 A.; Clark, S. B.; Tkachev, V. V.; Myasoedov, B. F. Colloid Transport of Plutonium in the Far-  
685 Field of the Mayak Production Association, Russia. *Science* (80-. ). **2006**, 314 (5799), 638–641.  
686 <https://doi.org/10.1126/science.1131307>.
- 687 (103) Dittrich, T. M.; Boukhalfa, H.; Ware, S. D.; Reimus, P. W. Laboratory Investigation of the  
688 Role of Desorption Kinetics on Americium Transport Associated with Bentonite Colloids. *J.*  
689 *Environ. Radioact.* **2015**, 148, 170–182. <https://doi.org/10.1016/j.jenvrad.2015.07.001>.
- 690 (104) Mesbah, A.; Szenknect, S.; Clavier, N.; Lozano-Rodriguez, J.; Poinssot, C.; Den Auwer, C.;  
691 Ewing, R. C.; Dacheux, N. Coffinite,  $\text{USiO}_4$ , Is Abundant in Nature: So Why Is It So Difficult to  
692 Synthesize? *Inorg. Chem.* **2015**, 54 (14), 6687–6696. <https://doi.org/10.1021/ic502808n>.
- 693 (105) Konings, R. J. M.; Beneš, O.; Kovács, A.; Manara, D.; Sedmidubský, D.; Gorokhov, L.;  
694 Iorish, V. S.; Yungman, V.; Shenyavskaya, E.; Osina, E. The Thermodynamic Properties of the f-  
695 Elements and Their Compounds: Part 2. The Lanthanide and Actinide Oxides. *J. Phys. Chem. Ref.*  
696 *Data* **2014**, 43 (1). <https://doi.org/10.1063/1.4825256>.
- 697 (106) Dorogova, M.; Navrotsky, A.; Boatner, L. A. Enthalpies of Formation of Rare Earth  
698 Orthovanadates,  $\text{REVO}_4$ . *J. Solid State Chem.* **2007**, 180 (3), 847–851.  
699 <https://doi.org/10.1016/j.jssc.2006.12.001>.
- 700 (107) Polinski, M. J.; Garner, E. B.; Maurice, R.; Planas, N.; Stritzinger, J. T.; Parker, T. G.;  
701 Cross, J. N.; Green, T. D.; Alekseev, E. V.; Van Cleve, S. M.; Depmeier, W.; Gagliardi, L.;  
702 Shatruk, M.; Knappenberger, K.L.; Liu, G.; Skanthakumar, S.; Soderholm, L.; Dixon, D.A.;  
703 Albrecht-Schmitt, T.E. Unusual Structure, Bonding and Properties in a Californium Borate. *Nat.*  
704 *Chem.* **2014**, 6 (5), 387–392. <https://doi.org/10.1038/nchem.1896>.
- 705 (108) Mazeina, L.; Ushakov, S. V.; Navrotsky, A.; Boatner, L. A. Formation Enthalpy of  $\text{ThSiO}_4$   
706 and Enthalpy of the Thorite  $\rightarrow$  Huttonite Phase Transition. *Geochim. Cosmochim. Acta* **2005**, 69  
707 (19), 4675–4683. <https://doi.org/10.1016/j.gca.2005.03.053>.
- 708 (109) Estevenon, P.; Kaczmarek, T.; Rafiuddin, M. R.; Welcomme, E.; Szenknect, S.; Mesbah,  
709 A.; Moisy, P.; Poinssot, C.; Dacheux, N. Soft Hydrothermal Synthesis of Hafnon,  $\text{HfSiO}_4$ . *Cryst.*  
710 *Growth Des.* **2020**. <https://doi.org/10.1021/acs.cgd.9b01546>.
- 711 (110) Suchanek, W. L.; Riman, R. E. Hydrothermal Synthesis of Advanced Ceramic Powders.  
712 *Adv. Sci. Technol.* **2006**, 45, 184–193.
- 713 (111) Weber, W. J.; Ewing, R. C.; Catlow, C. R. A.; Diaz De La Rubia, T.; Hobbs, L. W.;  
714 Kinoshita, C.; Matzke, H.; Motta, A. T.; Nastasi, M.; Salje, E. K. H.; Vance, E.R.; Zinkle, S.J.  
715 Radiation Effects in Crystalline Ceramics for the Immobilization of High-Level Nuclear Waste  
716 and Plutonium. *J. Mater. Res.* **1998**, 13 (6), 1434–1484. <https://doi.org/10.1557/JMR.1998.0205>.
- 717 (112) Weber, W. J.; Ewing, R. C.; Wang, L. M. The Radiation-Induced Crystalline-to-Amorphous  
718 Transition in Zircon. *J. Mater. Res.* **1994**, 9 (3), 688–698. <https://doi.org/10.1557/JMR.1994.0688>.
- 719 (113) Murakami, T.; Chakoumakos, B. C.; Ewing, R. C.; Lumpkin, G. R.; Weber, W. J. Alpha-  
720 Decay Event Damage in Zircon. *Am. Mineral.* **1991**, 76, 1510–1532.
- 721 (114) Ewing, R. C. Displaced by Radiation. *Nature* **2007**, 445 (January).
- 722 (115) Weber, W. J. Self-Radiation Damage and Recovery in Pu-Doped Zircon. *Radiat. Eff.*  
723 *Defects Solids* **1991**, 115 (4), 341–349. <https://doi.org/10.1080/10420159108220580>.
- 724 (116) Farnan, I.; Cho, H.; Weber, W. J. Quantification of Actinide  $\alpha$ -Radiation Damage in  
725 Minerals and Ceramics. *Nature* **2007**, 445 (7124), 190–193. <https://doi.org/10.1038/nature05425>.
- 726 (117) Robie, Richard A.; Hemingway, B. S. Thermodynamic Properties of Minerals and Related  
727 Substances at 298.15 K and 1 Bar ( 105 Pascals) Pressure and at Higher Temperatures. *U.S. Geol.*  
728 *Surv. Bull.* **1995**, 2131.
- 729 (118) Navrotsky, A.; Ushakov, S. V. Materials Fundamentals of Gate Dielectrics; **2005**.  
730 <https://doi.org/10.1007/1-4020-3078-9>.

731